Available online at www.sciencedirect.com
ScienceDirect
Journal of the European Ceramic Society 30 (2010) 2387–2395
www.elsevier.com/locate/jeurceramsoc

Oxidation resistance and strength retention of ZrB_2–SiC ceramics

Wei-Ming Guo, Guo-Jun Zhang *

State Key Laboratory of High Performance Ceramics and Superfine Microstructures, Shanghai Institute of Ceramics, Chinese Academy of Sciences, Shanghai 200050, China

Available online 4 March 2010

Abstract

Oxidation behavior and effect of oxidation on the room-temperature flexural strength were investigated for ZrB_2–10 vol% SiC (ZB10S) and ZrB_2–30 vol% SiC (ZB30S) in air at 1500 °C with times ranging from 0.5 h to 10 h. The oxide scale of both ZB10S and ZB30S was composed of an outer glassy layer and an inner extended SiC-depleted layer. The changes in weight gain, glass layer thickness, and extended SiC-depleted layer thickness with oxidation were measured. Analysis suggested that the extended SiC-depleted layer was most indicative for evaluating the oxidation resistance. Compared to the ZB10S, the improved oxidation resistance in ZB30S was attributed to the viscosity increase of glassy layer and the lower number of ZrO_2 inclusions in the glassy layer. Because of the healing of surface flaws by the glassy layer, the strength increased significantly by ∼110% for ZB10S and by ∼130% for ZB30S after oxidation for 0.5 h.

Keywords: B. Microstructure; C. Strength; ZrB_2–SiC; Oxidation; Kinetics

1. Introduction

Among ultra high-temperature ceramics (UHTCs), ZrB_2 has a desirable combination of low theoretical density, high melting temperature and thermal conductivity, which makes it attractive for use in thermal protection systems and scramjet engine components for hypersonic flight vehicles.[1] When ZrB_2 is exposed to air at high temperatures, it reacts with O_2 to form ZrO_2 and B_2O_3:

$$ZrB_2 + \frac{5}{2}O_2 \rightarrow ZrO_2 + B_2O_3(l) \quad (1)$$

Due to high vapor pressure, the B_2O_3 evaporates above 1100 °C[2]:

$$B_2O_3(l) \rightarrow B_2O_3(g) \quad (2)$$

The removal of B_2O_3 by vaporization leaves behind a porous ZrO_2 scale, which results in the rapid linear oxidation kinetics above 1400 °C.[3] Thus, the high-temperature applications of monolithic ZrB_2 will be limited by its poor oxidation resistance.

The addition of SiC has been reported to improve the oxidation resistance of ZrB_2.[3–5] Above 1100 °C, SiC reacts with O_2 according to the following reaction:

$$SiC + \frac{3}{2}O_2 \rightarrow SiO_2(l) + CO(g) \quad (3)$$

The SiO_2 and B_2O_3 form a borosilicate liquid, which covers the exposed surfaces. As temperature increases, B_2O_3 is continuously removed from the borosilicate liquid, leading to the formation of a SiO_2-rich glassy layer. Because SiO_2 is significantly less volatile and more viscous than B_2O_3, the SiO_2-rich layer provides effective oxidation protection for ZrB_2–SiC above 1100 °C.[5]

In the past 5 years, groups in the United States, Italy and China have investigated the oxidation behavior of ZrB_2–SiC ceramics.[2–12] Fahrenholtz et al. have studied the structure of oxide scales on ZrB_2–SiC ceramics after oxidation at temperatures up to 1500 °C.[3,5,6] They indicated that the typical scale is composed of three layers: (1) a SiO_2-rich glassy layer; (2) a thin ZrO_2–SiO_2 layer; (3) a SiC-depleted layer.[5,6] The development of the layered structure was analyzed with the aid of a thermodynamic model that involved volatility diagrams for ZrB_2 and SiC.[6] The model suggested that the formation of the SiC-depleted layer was due to the active oxidation of SiC under the oxide scale.[6] Similarly, Carney et al. showed that the oxide scale of ZrB_2–SiC ceramics after oxidation at temperatures ranging from 1400 °C to 1600 °C in air was again composed of three layers, where the third inner layer was constituted by a ZrO_2

* Corresponding author. Tel.: +86 21 52411080; fax: +86 21 52413122.
E-mail address: gjzhang@mail.sic.ac.cn (G.-J. Zhang).

0955-2219/$ – see front matter © 2010 Elsevier Ltd. All rights reserved.
doi:10.1016/j.jeurceramsoc.2010.01.028

matrix enclosing partially oxidized ZrB_2 with Si–C–B–O glass inclusions.[12]

Oxidation studies conducted by Karlsdottir et al. have focused on the surface features of the outermost glassy layer of ZrB_2–SiC ceramics that were oxidized at 1550 °C in air.[7–9] Island-in-lagoon patterns were observed on oxide scales, consisting of a central ZrO_2 "island" in a SiO_2-rich "lagoon". These oxide-scale features were called convection cells because of their role in transporting the B_2O_3-rich liquid to the surface where the B_2O_3 was lost by evaporation, and ZrO_2 precipitated from the remaining SiO_2-rich liquid. Additionally, the effect of SiC content on the formation of convection cell features was studied, showing that fewer convection cells formed and they were less uniformly distributed for ZrB_2–SiC with higher SiC content.[9]

The strength of non-oxide ceramics is affected by the oxidation process. To better drive high-temperature engineering applications of non-oxide ceramics, an understanding of the effects of oxidation on the room-temperature flexural strength of the material is essential. Considerable studies have reported strength retention for SiC and Si_3N_4 ceramics after oxidation,[13,14] but only limited experimental work involves strength retention of ZrB_2-based ceramics after oxidation.[15,16] Guo et al. compared the flexural strength of ZrB_2–SiC composites with nano-sized or micro-sized SiC particles before and after oxidation in dry air at 1400 °C for 10 h.[16] After oxidation, the flexural strength increased for ZrB_2–SiC containing nano-sized SiC particles, whereas the strength of the ZrB_2–SiC with micro-sized SiC particles decreased.[16]

In the present work, the oxidation behavior was studied for ZrB_2–SiC ceramics containing 10 vol% and 30 vol% SiC in air at 1500 °C for 0.5–10 h. Firstly, the microstructural features after oxidation were reported and discussed. Then oxidation kinetics was analyzed on the basis of weight gain, glass layer thickness and the extended SiC-depleted layer thickness. This work attempts to determine the most suitable parameter for oxidation resistance evaluation. In addition, the effect of oxidation time on the room-temperature flexural strength is also studied.

2. Experimental procedure

The raw materials used were ZrB_2 ($D_{10} = 0.46\,\mu m$, $D_{90} = 22.4\,\mu m$, 98.5%, Gongyi Sanxing Ceramics Materials Co. Ltd., Gongyi, China) and SiC ($D_{10} = 0.18\,\mu m$, $D_{90} = 1.0\,\mu m$, 98.5%, Changle Xinyuan Carborundum Micropowder Co. Ltd., Changle, China). In this paper, ZrB_2–SiC composites containing 10 vol% and 30 vol% SiC are referred to as ZB10S and ZB30S. The starting powder mixtures were ball milled for 8 h in acetone using Si_3N_4 balls in a planetary ball mill in nylon containers, and dried by rotary evaporation. Powder compacts were hot pressed at 2000 °C for 60 min under a pressure of 30 MPa. At temperatures below 1650 °C, the furnace was heated under vacuum. Above 1650 °C, the atmosphere was switched to flowing argon gas. A heating rate of ~10 °C/min was used between room temperature and 2000 °C. The furnace was cooled at a rate of ~20 °C/min.

Bars with dimensions of 2 mm × 2.5 mm × 39 mm were cut from the hot-pressed billets and ground to a 5 μm surface finish for oxidation testing. Oxidation studies were conducted in a box furnace. The samples were placed on alumina plate with minimal contact area. For evaluating whether the formed glassy layer is fluid at the set oxidation temperature, the specimens were tilted as shown in Fig. 1. The oxidation of the hot-pressed materials was conducted at 1500 °C for 0.5 h, 3 h and 10 h in stagnant air and the heating rate was 10 °C/min. Weights before and after oxidation were measured using a balance with 0.1 mg precision. The weight change results were an average of three bars.

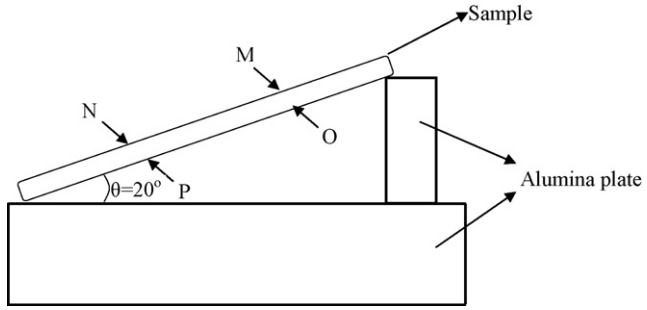

Fig. 1. Schematic of the specimen configuration for oxidation testing. Four sites (M and N on the top; O and P on the bottom) were at the one-third of length of specimen.

The hot-pressed and oxidized specimens were cut and polished for microstructure observation. Microstructures were characterized using scanning electron microscopy (SEM) imaging in an electron probe microanalyzer (JEOL JXA-8100F, Japan) along with energy-dispersive spectroscopy (EDS, Oxford INCA energy) for chemical analysis. Flexural strength of the as sintered bars and oxidized bars was determined via three-point bending with a span of 30 mm at a crosshead speed of 0.5 mm/min. For each composition and oxidation time, three specimens were tested.

3. Results

3.1. Microstructures of hot-pressed ZrB_2–SiC ceramics

Fig. 2 shows the microstructures of full dense ZB10S and ZB30S after hot pressing. Some pits (similar appearance to pores) were apparent in the micrographs as a consequence of particle pullout during polishing. The SiC particles (black phase) were well-distributed within the ZrB_2 (gray phase) matrix, and were primarily located at ZrB_2 grain junctions. The SiC particles tended to be isolated in ZB10S, but had a more interconnected appearance in the ZB30S. The ZrB_2 grain size of ZB10S was ~3.3 μm, whereas that of ZB30S decreased to ~2.2 μm. This showed that SiC particles inhibited the grain growth of ZrB_2 during hot pressing and the effect was stronger as the volume fraction of SiC increased.

3.2. Oxidation behavior and kinetics of ZrB_2–SiC ceramics

Fig. 3 presents mass gain per unit surface area as a function of oxidation time at 1500 °C for ZB10S and ZB30S. With increasing oxidation time, mass gain increased for both ZB10S and ZB30S. At identical oxidation time, the mass gain of ZB10S

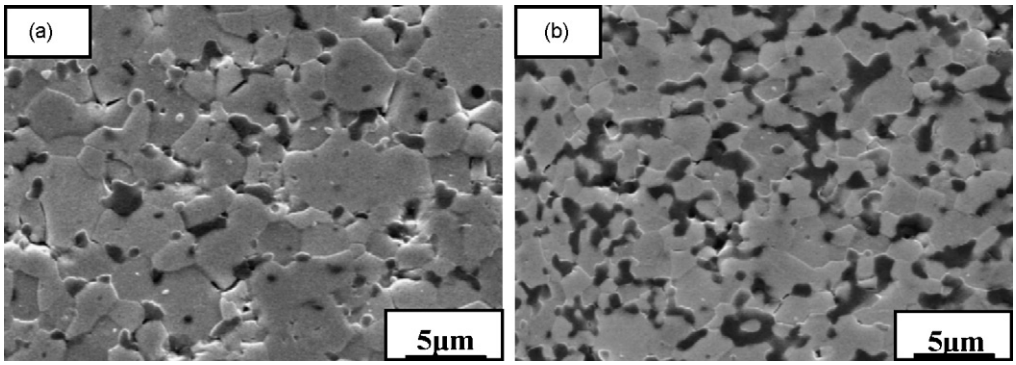

Fig. 2. Microstructures of hot-pressed ZrB_2–SiC composites: (a) ZB10S and (b) ZB30S.

was higher than that of ZB30S. For example, the mass gain of ZB10S after oxidation for 10 h was ~17.2 mg/cm^2, whereas the mass gain of ZB30S was only ~6.3 mg/cm^2.

To understand the effect of oxidation at different points on the sample, four sites (M, N, O and P in Fig. 1) on the top and bottom of a bar were chosen for microstructural analysis. The glassy layer thickness at M was similar with that of N, and the glassy layer thickness at O was close to that at P. This implies that the inclination of about 20° has no effect on oxidation. However, the glassy layer thickness of the top of the sample was different from that of the bottom. The glassy layer thickness for the top and bottom of oxidized ZB30S was measured by SEM imaging (Fig. 4). As expected, the glass layer thickness increased with oxidation time on the top of the sample. However, on the bottom, the glass layer thickness first increased and then decreased slightly with oxidation time. Additionally, the glassy layer on the bottom was thicker than that on the top after oxidation for 0.5 h and 3 h.

To better understand the oxidation behavior, the microstructure of the top of the bars was further analyzed. Figs. 5 and 6 show the backscattered electron (BSE) images and compositional maps of top of ZB10S ceramics after oxidation at 1500 °C for 0.5 h and 10 h. Figs. 7 and 8 show the BSE images and compositional maps of top of ZB30S ceramics after oxidation at 1500 °C for 0.5 h and 10 h. Even with 10 vol% SiC, an outer glassy layer was formed. However, the glassy layers on ZB10S and ZB30S had different microstructural features. ZrO_2 inclusions were observed in the glassy layer on ZB10S, whereas very few ZrO_2 inclusions were found in the glassy layer on ZB30S. With increasing oxidation time, the size and amount of ZrO_2 inclusions increased. After oxidation for 0.5 h, the size of ZrO_2 inclusions on ZB10S was in the range of 1–2 μm. When the oxidation time increased to 10 h, the ZrO_2 inclusions grew to 5–15 μm and became rod-shaped.

Despite differences in the oxide layer thickness, both ZB10S and ZB30S had similar layered structures in their oxide scales. According to previous studies,[5,6] the oxide scale of ZrB_2–SiC can be divided into three layers, as mentioned before. However, the ZrO_2–SiO_2 layer was usually very thin, so it was analyzed along with the SiC-depleted layer as one layer called the extended SiC-depleted layer. Therefore, the oxide scale for ZB10S and ZB30S consisted of two layers: (1) an outer glassy layer and (2) an inner extended SiC-depleted layer. Fig. 9 shows the thickness of the glassy layer and the extended SiC-depleted layer as a function of oxidation time for the ZB10S and ZB30S specimens at 1500 °C.

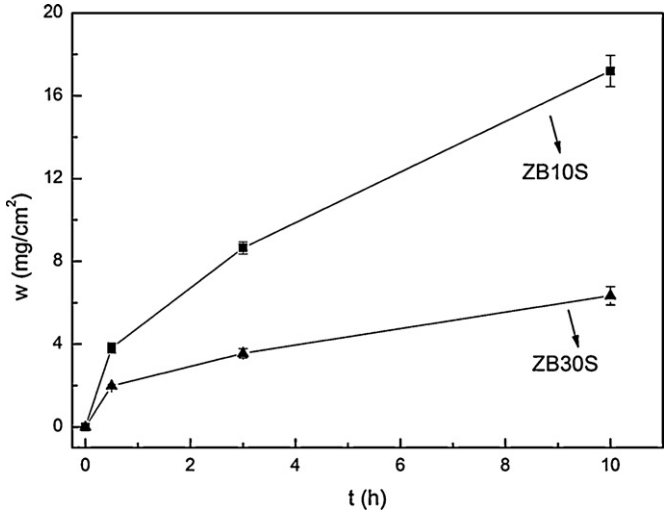

Fig. 3. Mass gain per unit surface area, w, as a function of oxidation time, t, for ZB10S and ZB30S at 1500 °C.

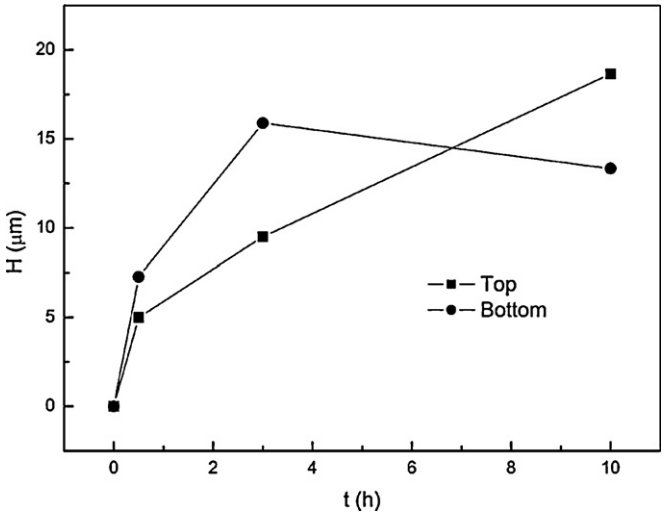

Fig. 4. Glassy layer thickness, H, on the top and bottom of ZB30S ceramics as a function of oxidation time, t, at 1500 °C.

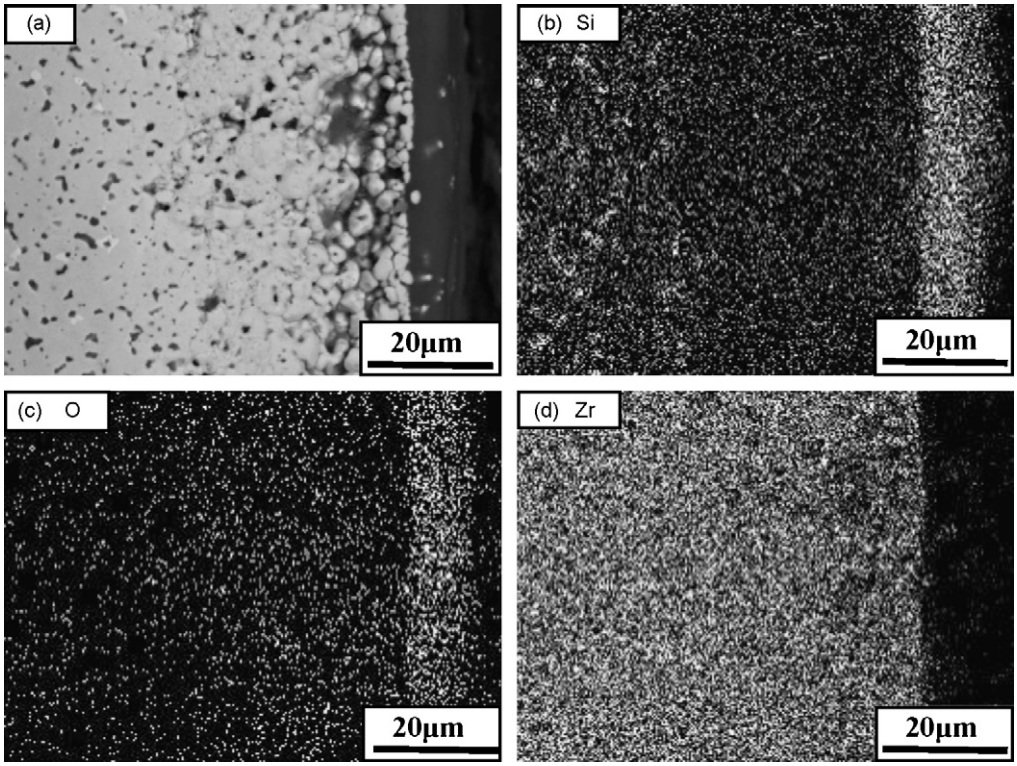

Fig. 5. Backscattered electron image (a) and compositional maps for (b) Si, (c) O, and (d) Zr of a polished section of ZB10S ceramic after oxidation at 1500 °C for 0.5 h.

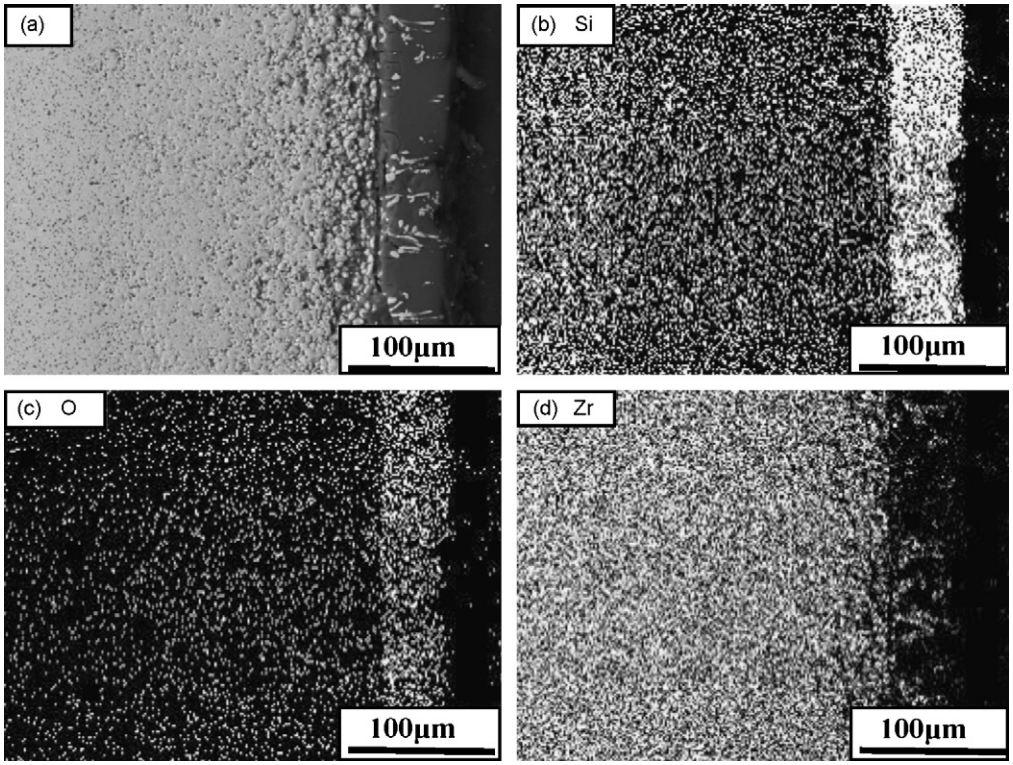

Fig. 6. Backscattered electron image (a) and compositional maps for (b) Si, (c) O, and (d) Zr of a polished section of ZB10S after oxidation at 1500 °C for 10 h.

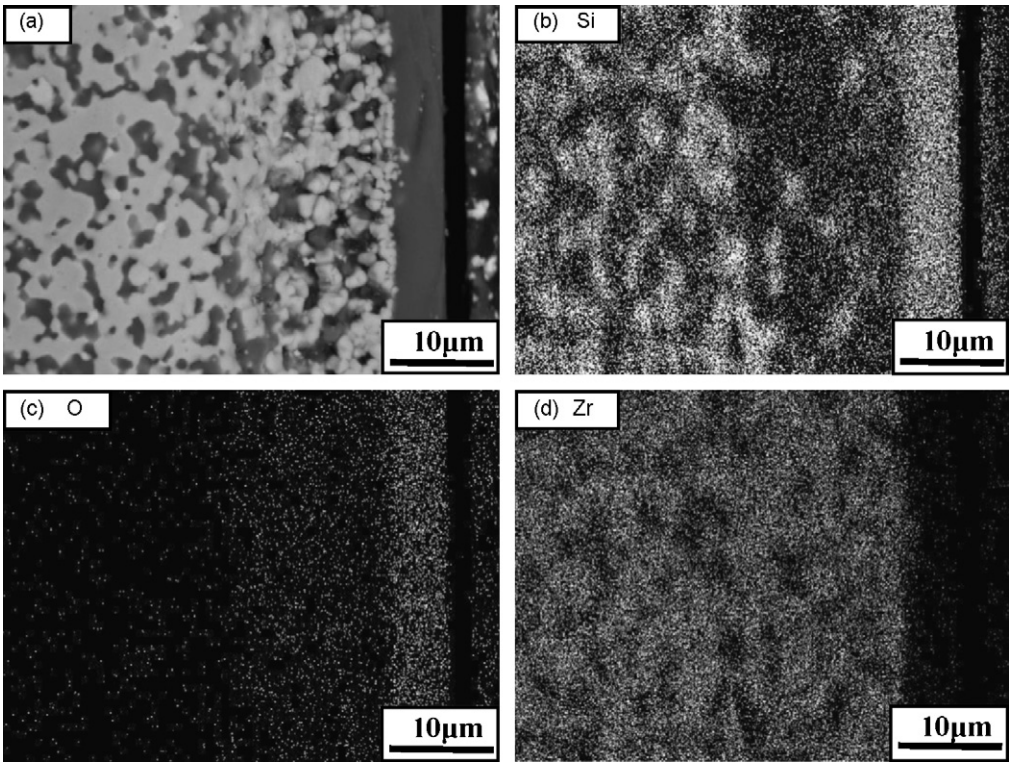

Fig. 7. Backscattered electron image (a) and compositional maps for (b) Si, (c) O, and (d) Zr of a polished section of ZB30S after oxidation at 1500 °C for 0.5 h.

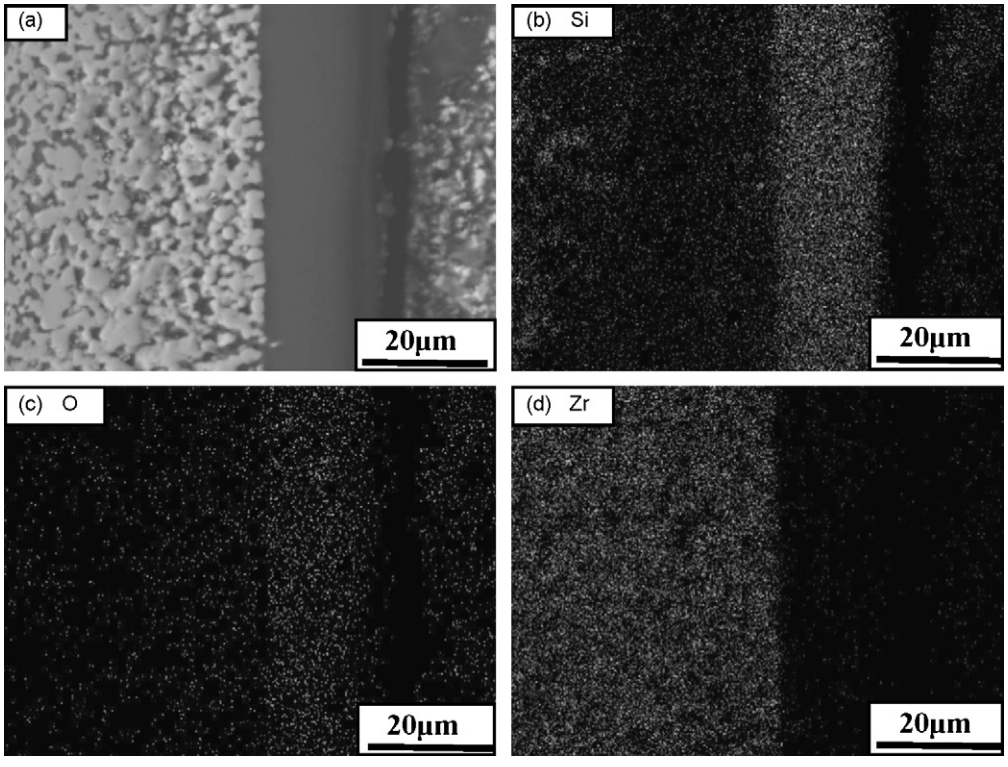

Fig. 8. Backscattered electron image (a) and compositional maps for (b) Si, (c) O, and (d) Zr of a polished section of ZB30S after oxidation at 1500 °C for 10 h.

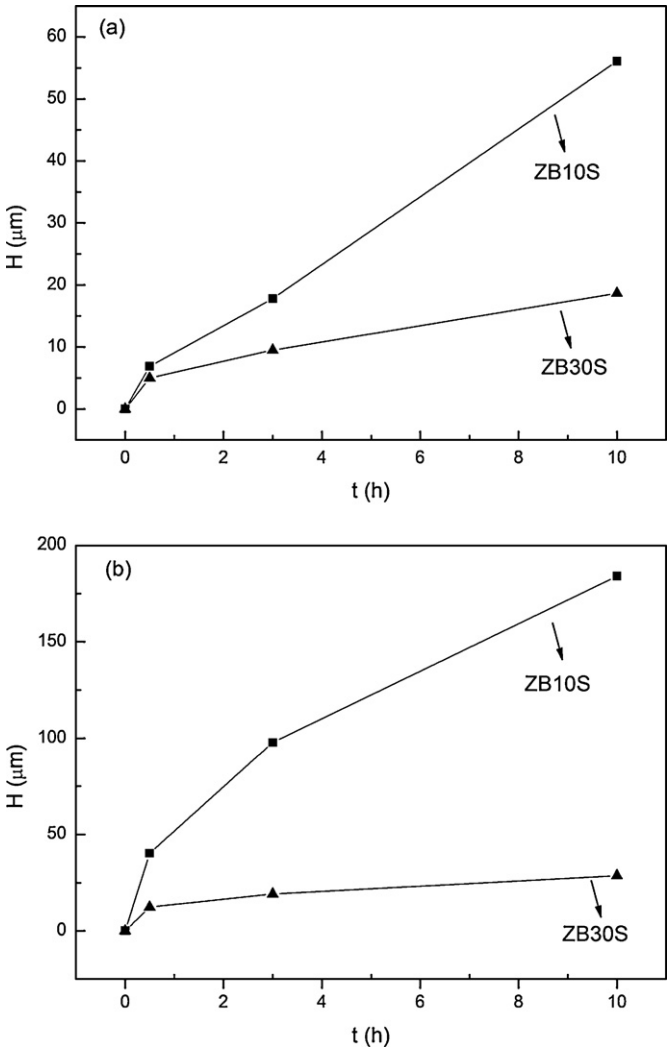

Fig. 9. Thickness of the glass layer (a) and extended SiC-depleted layer (b) on the top surface as a function of oxidation time at 1500 °C.

Combining the mass gain data with the glassy layer thicknesses and the extended SiC-depleted layer thicknesses from Figs. 3 and 9, the oxidation kinetics were analyzed for ZB10S and ZB30S using a generalized power rate equation[17,18]:

$$x^n = kt \quad (4)$$

where x is the change in mass or thickness, n is the exponent, k is the rate constant and t is the oxidation time. The kinetic parameters (n, k) and correlation coefficients (R) are listed in Table 1. Fitting of the kinetic data was good, as indicated by the values of the correlation coefficients ($R > 0.99$). According to the weight gain data, the oxidation of ZB10S and ZB30S followed parabolic kinetics. Using the glassy layer thickness data, the oxidation of ZB10S exhibited linear kinetics, whereas the oxidation of ZB30S still represented parabolic kinetics. Based on the extended SiC-depleted layer thickness data, the oxidation of ZB10S followed parabolic kinetics, whereas the oxidation of ZB30S followed cubic kinetics. Determination of which data are most suitable for evaluating the oxidation behavior is discussed in Section 4.3.

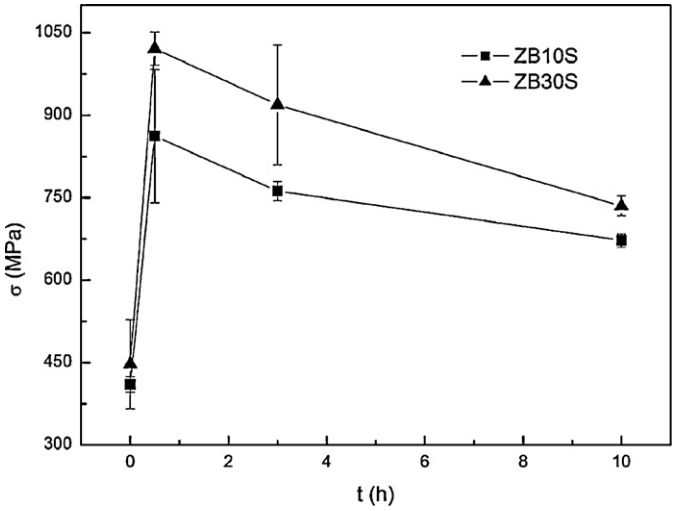

Fig. 10. Effect of oxidation time at 1500 °C on the room-temperature flexural strength of ZB10S and ZB30S.

3.3. Strength retention of ZrB_2–SiC ceramics after oxidation

Oxidation influenced the strength of ZrB_2–SiC ceramics (Fig. 10). As oxidation progressed, the retained flexural strength of ZB10S and ZB30S had similar trends. After 0.5 h, the flexural strength increased sharply, and then gradually decreased for longer times. However, the strengths of ZB10S and ZB30S after oxidation for 10 h were still higher than that of the unoxidized specimens.

4. Discussion

4.1. Microstructural features of oxidized ZrB_2–SiC ceramics

The glassy layer on the top and bottom of oxidized ZS30S differed in thickness and evolution (Fig. 4). As the temperature

Table 1
Best-fitting kinetic parameters, n, k, and correlation coefficients, R, for of the oxidation of ZB10S and ZB30S based on weight gain, glassy layer and extended SiC-depleted layer growth.

Sample	Weight gain			Glassy layer			Extended SiC-depleted layer		
	n	K ($(\mathrm{mg\,cm^{-2}})^n\mathrm{h^{-1}}$)	R	n	K ($\mu\mathrm{m}^n\,\mathrm{h^{-1}}$)	R	n	K ($\mu\mathrm{m}^n\,\mathrm{h^{-1}}$)	R
ZB10S	2	29.7	0.9987	1	5.4	0.9976	2	3.4×10^3	0.9998
ZB30S	2	3.9	0.9990	2	34.6	0.9984	3	2.3×10^3	0.9995

Table 2
Degree of material damage induced by oxidation in ZB10S and ZB30S at 1500 °C in air, assuming uniform oxidation within a sample.

Sample	Degree of material damage (%)		
	1 h	3 h	10 h
ZB10S	7.1	16.8	30.4
ZB30S	2.2	3.4	5.1

increases, the viscosity of glassy layer should decrease rapidly, allowing the glass to flow due to gravity. The flow of glass would result in a non-uniform thickness of the glassy layer, and consequently affect the oxidation behavior. A previous study showed that gravity influenced glass flow at 1400 °C and 1500 °C, but that the effect was greater at 1600 °C.[12] In the present study, SEM observation showed that the glassy layer on the top or bottom of oxidized ZS30S was uniform, indicating that the effect of gravity was small for an angle of 20°. So, in the present work, the effect of glass flow induced by the gravity on oxidation was ignored in the present analysis. The obvious difference in the glassy layer on the top and bottom of oxidized ZS30S was mainly attributed to the different local partial pressure. As shown in Fig. 1, the space between the bottom of the sample and the alumina plate was narrow. As the temperature reached 1500 °C, the vapor pressure of B_2O_3 increased substantially, leading to its evaporation. The narrow gap between the sample bottom and alumina plate may have allowed B_2O_3 vapor to accumulate, which would suppress its evaporation. As a result, the glassy layer on bottom could remain thicker than the top for shorter times (0.5 h and 3 h). As oxidation progressed, the oxygen partial pressure in the gap between the sample bottom and alumina plate decreased as oxygen was consumed and gaseous oxidation products (CO and B_2O_3) filled the gap. Due to the stagnant atmosphere, oxygen flow on the bottom surface might have been constricted and this could be the reason why the glass layer thickness did not increase on the sample bottom for longer times (10 h).

ZrO_2 inclusions were observed in the glassy layer of ZB10S, but not in the glassy layer of ZB30S (Figs. 5–8). During oxidation at 1500 °C, B_2O_3 was removed from the surface of the glassy layer by evaporation. Since, oxidation is a dynamic process, newly formed B_2O_3 is expected to continuously dissolve into the glassy layer. So, the glassy layer should contain some B_2O_3 at any time during oxidation and any point through the glassy layer. Because ZB10S contained 90 vol% ZrB_2, oxidation of ZB10S would produce more B_2O_3 in comparison to ZB30S, which contained 70 vol% ZrB_2. So, the B_2O_3 concentration in glassy layer of ZB10S was higher than that of ZB30S. Based on the calculated isothermal section at 1500 °C of the ZrO_2–SiO_2–B_2O_3 phase diagram,[8] increasing the B_2O_3 content of a SiO_2–B_2O_3 liquid increases the ZrO_2 solubility in the resulting ZrO_2–SiO_2–B_2O_3 (BSZ) liquid. Combining the above analysis with the calculated phase diagram of the ternary ZrO_2–SiO_2–B_2O_3, it was concluded that the glassy layer of ZB10S dissolved more ZrO_2 compared with that of ZB30S. Karlsdottir et al. also showed that ZrB_2–20 vol% SiC and especially the ZrB_2–30 vol% SiC had less dissolved ZrO_2 compared with the ZrB_2–15 vol% SiC because of the lower B_2O_3 content in the glassy layers.[9] In the oxidized ZB10S, the ZrO_2 first dissolved into the SiO_2–B_2O_3 liquid to form a BSZ liquid at the inner side of the glassy layer. Then the BSZ liquid would flow toward the top of glassy layer. When the B_2O_3 was lost by evaporation at the outer surface, ZrO_2 precipitated from the BSZ liquid. As oxidation progressed, rod-shaped ZrO_2 inclusions 5–15 μm long grew in the glassy layer of ZB10S.

4.2. Oxidation resistance evaluation of ZrB_2–SiC ceramics

From Table 1, the oxidation of ZrB_2–SiC ceramics had different kinetic characteristics based on whether weight gain, glassy layer thickness, or the extended SiC-depleted layer thickness was considered. The question is which is the most suitable for evaluating the oxidation resistance. The criteria for selection should include: (1) the degree of material damage induced by oxidation and (2) a reasonable comparison of the oxidation resistance of ZrB_2–SiC with different SiC contents. The best analysis has to satisfy the two criteria simultaneously.

As shown in Fig. 4, the oxidation on the top and bottom surfaces of the samples was different. This evidences showed that the local environment was heterogeneous. In addition, evaporation of B_2O_3 in oxidized ZrB_2–SiC should depend on the glassy layer composition, thickness and viscosity. Therefore, even for samples with uniform oxidation, it is not correct to compare the oxidation resistance of ZrB_2–SiC with different SiC contents using weight gain data alone. Similarly, due to the uncertainty due of the evaporation of B_2O_3, it is not correct to evaluate the degree of material damage and compare the oxidation resistance of ZrB_2–SiC with different SiC contents based only on the thickness of the glassy layer. For example, after oxidation for 0.5 h, the glassy layer of the ZB10S was close to that of the ZB30S, whereas the extended SiC-depleted layer of the ZB10S was much extended than that of the ZB30S (Fig. 9).

With the assumption that ZrB_2 and ZrO_2 have a theoretical density, 1 unit volume of ZrB_2 upon oxidation only produced 1.1 unit volumes of ZrO_2. Because the glassy layer covered the outermost surface of the sample, the thickness of the extended SiC-depleted layer was approximately the thickness of the material damage induced by oxidation. So, it was suitable to evaluate the degree of materials damage induced by oxidation and compare the oxidation resistance of ZrB_2–SiC with different SiC contents using the extended SiC-depleted layer thickness. Now, assuming that a uniform oxidation occurs on all the surfaces of the specimen, the degree of damage of ZB10S and ZB30S could be estimated from the extended SiC-depleted layer thickness, as shown in Table 2. After oxidation for 10 h, the degree of material damage of ZB10S was about 30.4%, whereas that of ZB30S was only about 5.1%. By this measure, the degree of material damage in ZB30S after 10 h was less than in ZB10S after 0.5 h. Based on factors discussed above, the extended SiC-depleted layer can be considered the most suitable for evaluating the oxidation resistance of ZrB_2–SiC ceramics.

4.3. Oxidation kinetics and mechanism of ZrB_2–SiC ceramics

Based on the extended SiC-depleted layer thickness, the oxidation of the ZB10S followed parabolic kinetics, whereas the oxidation of the ZB30S exhibited cubic kinetics. Generally, the oxidation of ceramics with a protective oxide layer exhibits parabolic kinetics ($n = 2$), indicating a diffusion-controlled mechanism. However, when the oxygen diffusion rate through the protective oxide layer decreases, oxidation kinetics deviate from parabolic behavior, tending toward a logarithmic relationship with scale growth resulting in $n \gg 2$.[17,19] For example, oxidizing, annealing, and reoxidizing CVD SiC in situ at 1300 °C, Ogbuji reported that devitrification of the oxide scale caused a decrease in the oxidation rate by a factor of about 30. Oxidation kinetics showed a strong departure from parabolic behavior, and the value of n was in the range from 6 to 10.[20] Therefore, the increase in the value of n observed in the present study from 2 for ZB10S to 3 for ZB30S, indicated that the glassy layer in ZB30S was more protective than that of ZB10S. Hence, we conclude that ZB30S had better oxidation resistance.

After oxidation for 0.5 h, the glassy layer of the ZB10S was similar to that of the ZB30S. Increasing oxidation time from 0.5 h to 3 h resulted in an increase in the thickness of the extended SiC-depleted layer by ~58 μm for the ZB10S. For comparison, thickness of the extended SiC-depleted layer increased by ~7 μm for the ZB30S. Therefore, the glassy layer thickness was not the main factor that influenced the oxidation resistance. As discussed in Section 4.1, the B_2O_3 concentration of glassy layer in the ZB30S is lower than that of ZB10S. The lower B_2O_3 concentration induced the higher viscosity of glassy layer of the ZB30S, which should retard oxygen diffusion.[9] Moreover, the dramatic decrease in the number of ZrO_2 inclusions enhanced the protective effect of the glassy layer on ZB30S. Therefore, the better oxidation resistance of ZB30S was attributed to two factors: (1) the higher viscosity and (2) fewer ZrO_2 inclusions in the glassy layer.

4.4. Strength retention

The change in bending strength with oxidation time was similar in ZB10S and ZB30S. After oxidation for 0.5 h, the strength increased by ~110% for ZB10S and by ~130% for ZB30S (Fig. 10). An increase in strength after oxidation have been previously observed from silicon based ceramics such as SiC and Si_3N_4.[13,14] This increase was attributed to the formation of a thin, dense oxide layer that could heal the surface flaws resulting from sample processing and machining. Surface flaw healing was effective only when the oxide layer was dense and very thin. When the oxide layer became thicker, the flaw healing effect was counterbalanced by the generation of new defects, either within the oxide scale or at the interface between the oxide scale and bulk materials.[14] Therefore, after further oxidation for 10 h, the strength was reduced by ~20% for ZB10S and ZB30S (Fig. 10), but still, the strength was ~65% higher after oxidation at 1500 °C for 10 h compared to the room temperature values.

5. Summary

Oxidation behavior and the effect of oxidation on the room-temperature flexural strength were investigated for ZrB_2–SiC ceramics containing 10 vol% and 30 vol% SiC. After oxidation in air at 1500 °C for 0.5–10 h, the oxide scale was composed of an outer glassy layer and an inner extended SiC-depleted layer. The glassy layer on top and bottom of ZS30S specimens differed in the thickness and growth rate, which was attributed to local differences in the environments of the top and bottom of the specimens. ZrO_2 inclusions were found in the glassy layers of ZB10S, because in this specimen more B_2O_3 was produced during oxidation and the SiO_2–B_2O_3 liquid could dissolve a higher amount of ZrO_2. On the contrary, almost no ZrO_2 inclusions were observed in ZBS30. The changes in weight gain, glass layer thickness, and extended SiC-depleted layer thickness with oxidation were measured. According to each of these parameters, oxidation of ZrB_2–SiC ceramics showed different kinetic characteristics. The thickness of the extended SiC-depleted layer was approximately the thickness of the material damage induced by oxidation, which suggested that the extended SiC-depleted layer was the most suitable to evaluate the oxidation resistance. Based on thickness of the extended SiC-depleted layer, the oxidation of the ZB10S followed parabolic kinetics, while the oxidation of the ZB30S exhibited cubic kinetics, indicating that the oxidation resistance of ZB30S was better than that of ZB10S. The improved oxidation resistance in ZB30S was attributed to the viscosity increase of glassy layer and the lower number of ZrO_2 inclusions in the glassy layer. Because of the healing of surface flaws by the outer glassy layer, oxidation promoted an increase in strength. After oxidation for 0.5 h, the flexural strength increased significantly by ~110% for ZB10S and by ~130% for ZB30S. With further oxidation (3 h and 10 h), the flexural strengths decreased, indicating that a new population of defects was created within a thicker glassy layer.

Acknowledgments

This work was financially supported by the Chinese Academy of Sciences under the Program for Recruiting Outstanding Overseas Chinese (Hundred Talents Program), the National Natural Science Foundation of China (No. 50632070), and the Science and Technology Commission of Shanghai (No. 08520707800 and No. 09ZR1435500).

References

1. Fahrenholtz WG, Hilmas GE. Refractory diborides of zirconium and hafnium. *J Am Ceram Soc* 2007;**90**:1347–64.
2. Li J, Lenosky TJ, Först CJ, Yip S. Thermochemical and mechanical stabilities of the oxide scale of ZrB_2 + SiC and oxygen transport mechanisms. *J Am Ceram Soc* 2008;**91**:1475–80.
3. Rezaie A, Fahrenholtz WG, Hilmas GE. Oxidation of zirconium diboride-silicon carbide at 1500 °C at a low partial pressure of oxygen. *J Am Ceram Soc* 2006;**89**:3240–5.
4. Monteverde F, Bellosi A. Oxidation of ZrB_2-based ceramics in dry air. *J Electrochem Soc* 2003;**150**:B552–559.

5. Rezaie A, Fahrenholtz WG, Hilmas GE. Evolution of structure during the oxidation of zirconium diboride-silicon carbide in air up to 1500 °C. *J Eur Ceram Soc* 2007;**27**:2495–501.
6. Fahrenholtz WG. Thermodynamic analysis of ZrB_2–SiC oxidation: formation of a SiC-depleted region. *J Am Ceram Soc* 2007;**90**:143–8.
7. Karlsdottir SN, Halloran JW, Henderson CE. Convection patterns in liquid oxide films on ZrB_2–SiC composites oxidized at a high temperature. *J Am Ceram Soc* 2007;**90**:2863–7.
8. Karlsdottir SN, Halloran JW, Grundy AN. Zirconia transport by liquid convection during oxidation of zirconium diboride-silicon carbide. *J Am Ceram Soc* 2008;**91**:272–7.
9. Karlsdottir SN, Halloran JW. Oxidation of ZrB_2–SiC: influence of SiC content on solid and liquid oxide phase formation. *J Am Ceram Soc* 2009;**92**:481–6.
10. Monteverde F, Scatteia L. Resistance to thermal shock and to oxidation of metal diborides-SiC ceramics for aerospace application. *J Am Ceram Soc* 2007;**90**:1130–8.
11. Guo WM, Zhou XJ, Zhang GJ, Kan YM, Li YG, Wang PL. Effect of Si and Zr additions on oxidation resistance of hot-pressed ZrB_2–SiC composites with polycarbosilane as a precursor at 1500 °C. *J Alloys Compd* 2009;**471**:153–6.
12. Carney CM, Mogilvesky P, Parthasarathy TA. Oxidation behavior of zirconium diboride silicon carbide produced by the spark plasma sintering method. *J Am Ceram Soc* 2009;**92**:2046–52.
13. Kim HW, Kim HE, Song H, Ha J. Effect of oxidation on the room-temperature flexural strength of reaction-bonded silicon carbides. *J Am Ceram Soc* 1999;**82**:1601–4.
14. Park H, Kim HW, Kim HE. Oxidation and strength retention of monolithic Si_3N_4 and nanocomposite Si_3N_4-SiC with Yb_2O_3 as a sintering aid. *J Am Ceram Soc* 1998;**81**:2130–4.
15. Sciti D, Brach M, Bellosi A. Long-term oxidation behavior and mechanical strength degradation of a pressurelessly sintered ZrB_2–$MoSi_2$ ceramic. *Scripta Mater* 2005;**53**:1297–302.
16. Guo SQ, Yang JM, Tanaka H, Kagawa Y. Effect of thermal exposure on strength of ZrB_2-based composites with nano-sized SiC particles. *Compos Sci Technol* 2008;**68**:3033–40.
17. Thorley M, Banks R. Kinetics and mechanism of oxidation of silicon nitride bonded silicon carbide ceramic. *J Thermal Anal Calorim* 1994;**42**:811–22.
18. Wen CH, Wu TM, Wei WCJ. Oxidation kinetics of LaB_6 in oxygen rich conditions. *J Eur Ceram Soc* 2004;**24**:3235–43.
19. Nickel KG. Multiple law modelling for the oxidation of advanced ceramics and a model-independent figure of merit. In: Nickel KG, editor. *Corrosion of advanced ceramics-measurement and modelling*. Dordrecht (NL): Kluwer Academic Pub.; 1994. p. 59–72.
20. Ogbuji LUJT. Effect of oxide devitrification on oxidation kinetics of SiC. *J Am Ceram Soc* 1997;**80**:1544–50.